Research Square

Preprints are preliminary reports that have not undergone peer review.
They should not be considered conclusive, used to inform clinical practice,
or referenced by the media as validated information.

Improvement in barrier, mechanical and antioxidant properties depicted in rose petal extract (RPE)-incorporated nanocellulose and polyvinyl alcohol (PVA)-based food packaging films

Urvashi Singh
Indian Institute of Technology
Madan Kumar
Indian Institute of Technology
Vivek Kumar
Vivekkrdat@iitd.ac.in

Indian Institute of Technology
S. K. Khare
Indian Institute of Technology

Research Article

Keywords: Plastic pollution, biodegradable food packaging, nanocellulose, plant-based extract, barrier property.

Posted Date: November 19th, 2026

DOI: https://doi.org/10.21203/rs.3.rs-11272464/v1

License: This work is licensed under a Creative Commons Attribution 4.0 International License.
Read Full License

Additional Declarations: No competing interests reported.

Improvement in barrier, mechanical and antioxidant properties depicted in rose petal extract (RPE)-incorporated nanocellulose and polyvinyl alcohol (PVA)-based food packaging films

Urvashi Singh [a], Madan Kumar [a], Vivek Kumar [a *], S. K. Khare [b]

[a] Centre for Rural Development and Technology, Indian Institute of Technology, Delhi, India

[b] Department of Chemistry, Indian Institute of Technology, Delhi, India

Urvashithakur77@gmail.com, madankumar9052@gmail.com, Vivekkrdat@iitd.ac.in, skkhare@iitd.ac.in

[*]**Corresponding author details:**

Prof. Vivek Kumar

Professor

Centre for Rural Development and Technology

Indian Institute of Technology, Hauz Khas-110016, Delhi, India

E-mail: vivekk@rdat.iitd.ac.in

Tel: +919412619735

Abstract:

This article investigates the role of nanocellulose incorporated with plant-based extract in making biodegradable food packaging film and functional coating. The food sector is one of the largest industries using petroleum-based products for packaging, thus contributing to plastic pollution. This has raised the demand for bio-based packaging. Nanocellulose has been one of the important choices of materials for making biodegradable food packaging films, but due to its lack of barrier properties, its usage becomes a point of concern. Plant-based extracts have also been in research for a few decades, as they make a good choice of additives for enhancing the properties of natural biomaterials. Sugarcane bagasse was used for the extraction of cellulose and PVA was used as the crosslinking agent to cast the film. Nanoparticle tracking analysis (NTA) confirmed a size of around 135 nm for nanocellulose. RPE was used in blend with the matrix and as a coating over the cast PVA-CNC films. The results were compared based on barrier, mechanical, thermal and antioxidant properties. Contact angle was found to increase by around 25%, and there was an 80% improvement witnessed in the elongation % of the films with increasing RPE content. Films also displayed around 98% radical scavenging due to the presence of anthocyanins in RPE. Films with extract exhibited slow thermal degradation as compared with neat films.

Keywords

Plastic pollution, biodegradable food packaging, nanocellulose, plant-based extract, barrier property.

1. Introduction:

Plastic accumulation in our ecosystem has become a global issue as increasing amounts of plastic waste, especially from the food packaging industry, is being dumped into our water bodies and land in the form of landfills (Yogalakshmi & Singh, 2020). Single-use plastics are the major concern as these are discarded after a few uses and their disposal becomes a problem (Nagy & Kuti, 2016). These make up to 95 % of the total plastic used in packaging. This has led to an increasing need for biodegradable packaging. Food packaging polymers are broadly categorized into non-biodegradable and biodegradable. Non-biodegradable polymers are petroleum-based materials, majorly polyethylene terephthalate (PET), polyolefins (PO), polycarbonate (PC), polystyrene (PS), polyethylene naphthalate (PEN), polyvinyl chloride (PVC), ethylene vinyl alcohol (EVOH), polyamide (PA), polyethylene (PE), and polypropylene (PP) (Sharma et al., 2026). Biodegradable polymers, on the contrary, can be derived from natural sources or synthesised. Natural polymers are obtained from biomass, polysaccharides (cellulose, starch, agar, alginate, carrageenan), some from proteins (whey, soy, casein, gluten), lipids, as well as from microorganisms [polyhydroxyalkanoates (PHA) and polyhydroxybutyrate (PHB)]. Examples of synthetic biodegradable polymers include aliphatic polyester [polycaprolactone (PCL)], aromatic copolyesters [polybutylene adipate terephthalate (PBAT)] and aliphatic copolyesters [polybutylene succinate (PBS)].

Biodegradable polymers mainly derived from agricultural waste, specifically cellulose, lignin, and starch, are being explored for creating improved biodegradable films and coatings (Selvam et al., 2025). Cellulose, a natural polymer made up of D-glucose units, is hydrophilic and allows for extensive chemical modification. In food systems, it serves as a filler or stabiliser, enhancing stability, texture, and sensory qualities (He et al., 2021). Among food packaging polymers, cellulose and its derivatives are prevalent due to their biocompatibility, sustainability, low cost, mechanical strength, and biodegradability (Liu et al., 2021). However, limitations such as excessive water absorption and poor adhesion, along with inadequate mechanical strength and thermal/barrier properties, exist (Rhim & Ng, 2007). To address these issues, biopolymer composites are used to create barrier-enhancing packaging films. For instance, sodium caseinate and paraffin wax coatings on paper reduce water vapor transmission rates, making the paper smooth and moisture-resistant (Khwaldia, 2010); however, sodium caseinate is unsuitable for lactose-intolerant individuals. Additionally, whey protein coatings can improve oil barrier properties but may compromise tensile strength (J. H. Han & J. M. Krochta, 1999). Research has shown that treating kraft paper with citrus waste

enhances air and water barriers while imparting antioxidant properties (Kasaai & Moosavi, 2017) . Blending cellulose with naringin provides UV blocking, antioxidant, antibacterial effects, and hinders water vapor passage, though the concentration ratio must be optimized to maintain moisture resistance.

Nanocellulose, derived from cellulose, displays several properties due to a higher surface area to volume ratio, and is considered a good reinforcing material as it can be successfully incorporated with polymers like alginate, polycaprolactone, polyvinyl alcohol (PVA) and others to make environmentally stable composites (Chakrabarty & Teramoto, 2018). Nanocellulose is namely of two types, crystalline nanocellulose (CNC) and fibrillated nanocellulose (CNF) (Kusmono et al., 2020). The mechanical strength of CNC is comparable to that of steel (Phanthong et al., 2018) (Oksman & Sain, 2016) due to its high crystallinity. So, CNC has been used in films and as coatings to impart strength to the matrix (Khwaldia, 2010), (Guzman-Puyol et al., 2022), (Ji et al., 2020). Natural matrix materials like polylactic acid (PLA), poly-hydroxyalkanoates (PHA), polyhydroxybutyrate (PHB) and poly-vinyl alcohol (PVA) (Amara et al., 2021) are explored to reinforce the films. PVA is a water-soluble, biodegradable synthetic polymer. It promotes better crosslinking of polymer chains due to its excessive hydroxyl groups. There are several works that depict the effectiveness of PVA/CNC together as a film-forming matrix (Popescu, 2017). According to research, novel PVA/CNC/TiO_2 nanocomposites were successfully developed, characterised, and demonstrated as promising materials for food packaging. These composites exhibit strong antibacterial activity, excellent mechanical strength, superior UV-shielding ability, and efficient water vapour barrier properties (Ulaganathan et al., 2022).

Plant-based extracts, natural polymers, and plasticisers are being researched to enhance material properties. Key pigments like Chlorophyll (Chavoshizadeh et al., 2020), carotenoids (Kanatt et al., 2020), tannins (Lee et al., 2020), anthocyanins (Zhang et al., 2020), curcumin (Musso et al., 2017), betalains (Yao et al., 2020), brazilin and quercetin (Kurnianto et al., 2020; Masek et al., 2018) are abundant in plants and food materials. Tannins combined with cellulose nanofibers (CNF) enhance food packaging films, providing mechanical strength and hydrophobicity (Ghaderi et al., 2014). Although serving as an antioxidant, tannin is not thermally stable. Rose, being an ornamental flower, is usually wasted in large quantities (Hasan et al., 2015). The waste can be used to derive rose petal extract, which has proven to help develop smart packaging (Kanatt, 2021a). Rose petals possess superhydrophobic surfaces with waxes and lipids that prevent water penetration (Bhushan & Nosonovsky, 2010). (Kanatt, 2021a) research showed that food packaging films composed of CMC (carboxymethyl cellulose) and PVA with rose petal extract significantly decreased water solubility and swelling capacity. These films exhibited higher tensile strength compared to standard films. Shelf-life studies on fish demonstrated a reduction in food decay.

In contrast to CMC used by Kanatt (2021b), our work explores the film-forming properties of CNC to study how it behaves in the presence of PVA, while incorporating RPE in the blend and as a coating over neat PVA-CNC films to study and compare the improvement in properties. Solvent casting was explored to cast the RPE blended films and spray coating was employed to coat neat films. Along with barrier, mechanical and thermal analysis, antioxidant properties of the films were also explored.

2. Materials and Methods:

2.1. Materials

Sugarcane bagasse was obtained from Mohit Paper Mill, Bijnore. Rose petals were obtained from the IIT Delhi campus. Polyvinyl alcohol (PVA), M_w = 72000 was purchased from Merck Chemicals. Ortho-phosphoric acid (Molarity = 98gms/mol) was purchased from Merck Chemicals. Hydrogen peroxide (30 % w/v with MW= 34.1) and Sodium hydroxide pellets (M.W. = 40 g/mol) were purchased from Thermo Fisher. Citric acid anhydrous (M.W.= 192.12 g/mol) was purchased from Sigma Aldrich. ABTS (2,2′-azino-di-[3-ethylbenzthiazoline sulfonate), (MW= 548.68) and DPPH (2,2-diphenyl-1-picrylhydrazyl), (MW= 394.32) were purchased from Sigma Adlrich. Ethanol (MW=46.07) wasppurchased from Sigma Adlrich.

2.2. Preparation of solutions and films

2.2.1 Preparation of nanocellulose suspension and PVA solution

As shown in Fig. 1, sugarcane bagasse was first dried and milled to obtain a fine powder. Alkali treatment was given for 2 hours using 8% NaOH, followed by bleaching with 20% hydrogen peroxide (H_2O_2), which rendered an almost white powder, thus indicative of the removal of lignin. Then, acid hydrolysis was carried out with 5 M H_3PO_4 (optimized concentration after trying 2 M and 10 M) for around an hour at 55 °C, which completely removed the left-out lignin, hemicellulose and other components. This step is supposed to eliminate the amorphous regions completely so that the obtained product is highly crystalline. The white powder thus obtained is dissolved in water with continuous stirring for around 5 hours and then ultrasonicated for 60 minutes at 50% power via a probe sonicator. The suspension obtained is kept for an hour after sonication and then decanted to obtain a white transparent liquid. PVA solution was prepared at 5 % and 6 % concentrations via constant stirring at 80 °C for 2-3 hours till a transparent, clear liquid is obtained. This was stored at room temperature.

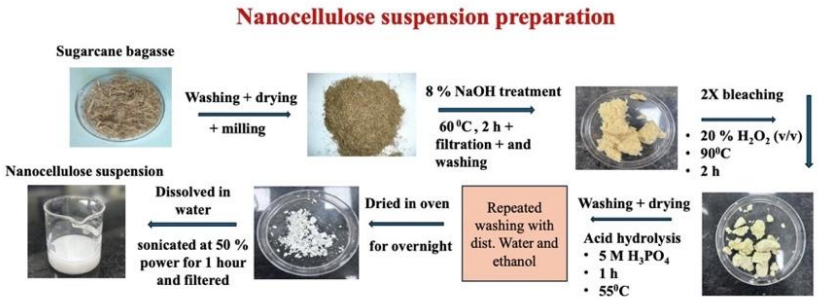


Fig 1: Preparation of nanocellulose suspension from sugarcane bagasse.

2.2.2 Preparation of PVA/CNC films

5% and 6% PVA and 1% and 2% CNC solutions were mixed well in the ratio 1:3 (optimised ratio) via continuous stirring at around 40 °C on a magnetic stirrer for 1.5-2 hours. Then the solution was left to sit at room temperature for 10 minutes, after which it was poured into 90 mm petri dishes after slight greasing with petroleum jelly. These petri dishes were then kept in an oven overnight to dry. Films were peeled off after 12 hours with the help of a twizzer and stored in a desiccator till further testing. 4 films were obtained with different compositions, with 5% PVA and 6% PVA films being the control films (without any additive). Table 1 shows how different ratios and concentrations of both the components were used to make 4 different films.

Table 1. Depicts ratios and concentrations of PVA and CNC incorporated to make films with different compositions

Films	PVA concentration	CNC concentration
5P1C	5%	1%
5P2C	5%	2%
6P1C	6%	1%
6P2C	6%	2%

2.2.3 Preparation of Rose petal extract

Rose petals were washed and dried in an oven for 12 hours at 70 °C. Once they turned yellow, they were crushed in a mixer, and the powder was put in a mixture of 0.1 M citric acid and 70% ethanol and placed in a shaker incubator at 150 rpm overnight. The solution thus obtained is filtered via vacuum filtration and the pink-colored solution thus

obtained after decanting is stored in cool conditions for further use. The solution is prepared at 5 % concentration after optimization. The process is shown in Fig. 2.

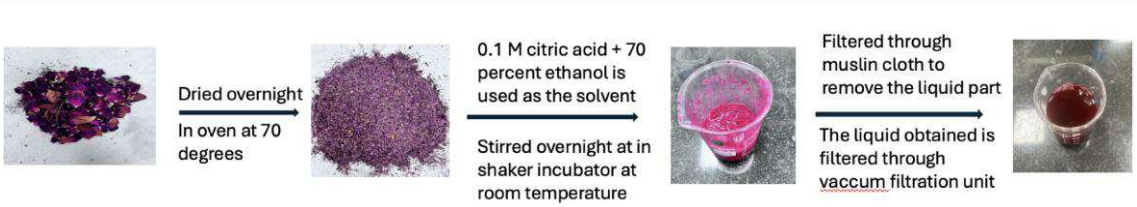
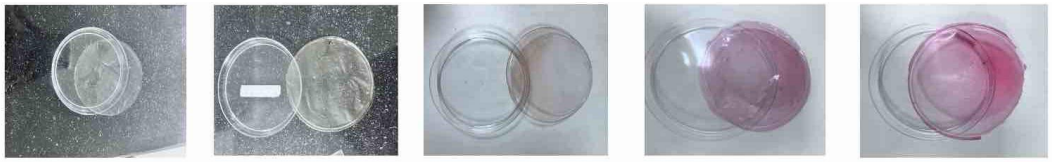


Fig 2: Step-by-step rose petal extract preparation

2.2.4 Film formation with RPE incorporation and coating

An optimised sample from different PVA-CNC films was chosen for further experiments. RPE was added to the matrix solution in different ratios and again stirred for 60 minutes at room temperature. The mixture obtained is cast in a volume of 15 ml in 90 mm petri dishes, after slight greasing. Petri dishes are kept at room temperature for 1 hour and then kept in an oven at 60 °C for 10-12 hours till they are completely dry. Films formed were peeled off and kept in a desiccator for further use. Fig.3. (a) shows the films with different RPE ratios. Films were coded as RPC=1:10, where 1:10 is the ratio of RPE: PVA-CNC matrix solution, and so on till RPC=1: 2. Spray coating was performed on neat PVA-CNC films with the help of a spray bottle. Single coating and triple coatings were done on different films. Once coated, the film was left to dry in an oven for 3-4 hours, and the coating was repeated. This was done thrice to achieve triple coating as shown in Fig. 3 (b).



(a)



(b)

Fig. 3. (a) Pictorial representation of control and test films starting from neat PVA, PVA-CNC film to films with increasing incorporation of RPE in blend; (b) PVA-CNC films with RPE coated in single layer and triple layers from left to right

2.3 Characterizations

2.3.1. Structural analysis

The internal bonding was studied via Fourier Transform Infrared Spectroscopy (FTIR Nicolet iS05) with a range lying between 4000–400 cm^{-1} and resolution set at 4 cm^{-1}.

Crystallinity was accessed using X-Ray Diffraction (XRD Empyrean Malvern PANalytical) available at IIT Delhi Sonipat campus. The diffraction intensities were recorded between 10°-85° for the films (2θ angle range) at a rate of 3° per minute. XRD and FTIR were performed for the nanocellulose suspension and films to assess changes in crystal structure and chemical bonding occurring between PVA and CNC and later with RPE

2.3.2 Morphological analysis for nanocellulose suspension

Transmission Electron Microscopy (TEM) was performed for the nanocellulose suspension with 120 KV TEM and TEMCON software was used for data processing. The liquid sample was first drop casted on TEM copper grids and dried for 5-6 hours before viewing under the microscope.

2.3.3 Particle size and distribution for nanocellulose suspension

Nanoparticle tracking analysis (NTA) was done via Nanosight version 3.4. Camera used for anaylysis was sCMOS set at 25 FPS with approx. 1500 frames. Blue488 lazer was used. Room temperature was employed for analysis with dilution factor of 1 x 10e0. Mean, mode and standard deviation was detected with concentration of the particles in particular frames for the suspension.

2.3.4 Mechanical properties

Tensile strength (TS) and elongation break (EB) of the films were measured according to ASTM 828-97 (ASTM E96/E96M-22: Standard Test Methods for Gravimetric Determination of Water Vapor Transmission Rate of Materials, 2022) using the Zwick roell z010 analyzer. Before testing, gauze length of 25 mm was used and 10 mm wide strips were cut from each film and fixed on the analyzer with a testing speed of 5 mm/s. The values were calculated according to the given equations

$$TS = F/x$$

$$EB = \Delta L/L_O \times 100$$

Where, F = maximum stretching strength; x = film thickness; ΔL = elongated length; L = original length of the sample.

2.3.5 Contact angle analysis

Hydrophobicity was checked using Drop Shape Analyser, DSA 25 (KRUSS GmbH, Germany) where in 1 μL of water droplet was placed on the sample at a speed of 0.2 μL /s which is positioned on the flat sample stage at room temperature. The pictures were taken at 150 fps frame rate.

2.3.6 Water Vapor Transmission Rate (WVTR)

Along with the contact angle test, barrier property for RPE incorporated films was also tested via WVTR. WVTR was performed using Permatran-W 3/34 Mocon and the OTR using Ox-tran 2/22 Mocon as per ASTM F1249 and ASTM D3985, respectively.

2.3.7 Antioxidant activity

DPPH and ABTS assays were performed for RPE films to test radical scavenging activity for different RPE content in the films. Total anthocyanin content (TAC) in RPE was estimated using the formula in Eq (1)

$$TAC\ \left(\frac{mg}{g}\right) = \frac{\mathrm{A}*\mathrm{DF}*\mathrm{M_W}}{\mathrm{L}*€} \quad (1)$$

Where,

$$A = (Abs_{520} - Abs_{700})_{pH1} - \left(Abs_{\{520\}} - Abs_{700}\right)_{pH4.5} \quad (2)$$

DF- dilution factor; M_W- molecular weight of anthocyanins (449.2 g/mol); €- molar extinction coefficient for anthocyanins (26900 L/cm/mol; L- cell width 2 cm).

RPE was diluted with 2 buffer solutions, separately, in the ratio 1:10 each, where 10 is buffer and 1 is RPE. Buffer 1 was a 0.025 M KCL solution at pH 1, and buffer 2 was a 0.4 M CH_3COONa solution at pH 4.5. The solutions were allowed to sit at room temperature for 15 minutes. OD was recorded at 520 nm and 700 nm for each solution. The absorbance was calculated as per Eq (2)

0.1mM DPPH was prepared by mixing the required amount in methanol. The solution has to be stored in the dark for 1 hour before use. Then, films of equal weight were completely immersed in 2 ml of DPPH and stored in the dark for 2 hours, after which UV was recorded at 517 nm in the spectrophotometer. The UV absorbance should be between 0.7-1 for DPPH solution. The percentage of inhibition for DPPH was calculated according to Eq (3)

$$\%\ inhibition = \frac{Abs_{\{DPPH\}} - Abs_{\{samples\}}}{Abs_{\{DPPH\}}} * 100 \quad (3)$$

A 0.007 M ABTS solution was prepared by dissolving the appropriate amount of ABTS reagent in water. This solution was then mixed with a 2.45 mM potassium persulfate solution in a 1:1 volume ratio and allowed to react for 1 hour. The resulting mixture was diluted with ethanol till the solution gave absorbance of around of 0.7-0.8 at 735 nm. 15 mg of each film was put into the 2 ml solution and incubated in the dark for 5 minutes. The absorbance was then measured at 735 nm using a UV–Vis spectrophotometer. Activity was calculated according to the formula in Eq (4)

$$\%\ inhibition = \frac{Abs_{control} - Abs_{sample}}{Abs_{control}} * 100 \quad (4)$$

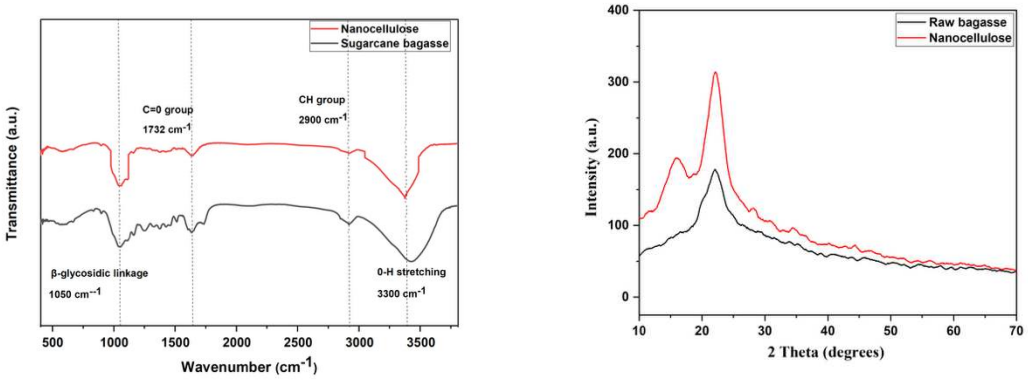
3. Results and discussions:

3.1 For nanocellulose suspension

3.3.1 Structural analysis

By identifying the functional groups that were present in the substrate both before and after treatments, FTIR was used to investigate the change in the chemical structure. As seen in Fig. 4 (a), the OH stretching vibration of the hydroxyl group in cellulose, hemicelluloses, and lignin is represented by a broad absorption band in the 3333–3342 cm^{-1} range that is observed for both the fibres (Gupta, 2020). But in the case of the treated sample, the peak is seen shifted towards a higher wavenumber due to changes in hydrogen bonding (due to increased crystallinity or nanoparticle formation) (Morán et al., 2008). Also, the peak is weaker in intensity and narrower due to the higher crystallinity of CNC and more uniformity in hydrogen bonding. The spectra of both types of fibers display an absorption band around the 2900 cm^{-1} region, which indicates the presence of cellulose, hemicellulose, and lignin's CH group. The untreated fibre's spectra show peaks at 1732 cm−1, which can be attributed to the C=O stretching vibration of the acetyl and uronic ester groups found in lignin and hemicelluloses. The reduction of this peak in nanocellulose suggests that lignin and hemicelluloses have been eliminated. The untreated fibre's peaks at 1238 cm^{-}

[1], 1370 cm^{-1}, and 1512 cm^{-1} are indicative of lignin's aromatic skeletal vibration. All these are eliminated in nanocellulose (Agarwal & Reiner, 2009). The most prominent absorption band, observed to increase from the untreated fibre to the nanocellulose, is the one at 1050 cm^{-1}, typical of β-glycosidic linkages between glucose units (Kotov et al., 2023).



(a) (b)

Fig. 4. (a) FTIR spectra for raw SCB and nanocellulose suspension; (b) XRD spectra of raw SCB and nanocellulose suspension.

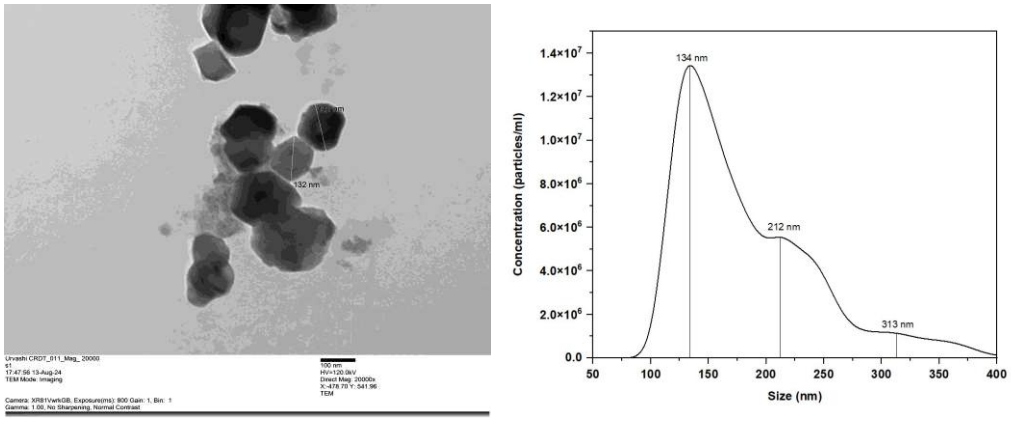
XRD was performed to examine the crystallinity of raw sugarcane bagasse and nanocellulose. Eq. (1) was used to determine crystallinity index I_C ; where $I_{2\theta}$ represents the peak at 22.5 °, and I_{am} represents peak at 18 °. $I_{2\theta}$ represents crystalline and amorphous regions of the sample and I_{am} represents the amorphous regions.

$$Ic = \frac{I_{2\theta}}{I_{2\theta} + I_{am}} * 100 \quad (1)$$

As we see in Fig. 4. (b), the peak at 18 ° has almost diminished in the treated sample and the peak at 22.5 ° has become narrower and sharper. This points out the fact that as we move from raw bagasse to nanocellulose, crystallinity has increased and all the amorphous regions have been removed. The crystallinity index of the SCB was calculated as 35.6%, and for nanocellulose, it came out to be 54 % (Ghazy et al., 2016)

3.3.2 TEM and particle size distribution

TEM images revealed how nanocellulose is dispersed in the suspension in the form of crystals. Distribution lies in nanometric range according to Fig 5.(a). At some locations, the crystals are agglomerated, and at others we can see individual crystals. 135 Nm and 141 Nm can be seen as the sizes of crystals, which indicate proper formation of a crystalline suspension



(a) (b)

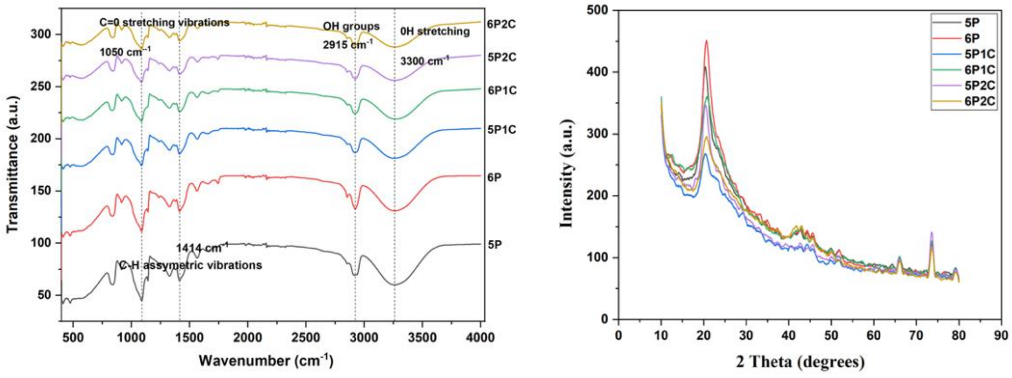
Fig. 5. (a) TEM showing formation of CNC with a size in the range of 135 nm; (b) NTA analysis for nanocellulose suspension

NTA results revealed the average particle size to be 189 nm, and the highest concentration of the particles was in the range of 135 nm. Fig. 5. (b) shows how the concentration of particles is decreasing with increasing size. The results coincide with TEM data showing average particle size lying in the same range (Jesús Dueñas-Mas et al., 2018).

3.2 For PVA-CNC films

3.2.1 Structural analysis

FTIR: All spectra show a broad band at about 3280 cm^{-1}, which is attributed to the OH groups' free O-H stretching vibrations. This band depicts intermolecular hydrogen bonding between the hydroxyl groups of PVA and the CNC as well as O-H stretching vibrations from intramolecular hydrogen bonds within the PVA (Popescu, 2017b). The incorporation of nanocellulose in PVA matrix causes a slight shift in the intensity of OH stretching. This may be due to the interface between the OH group on the surface of nanocellulose and the one in PVA. Nanocellulose and PVA have a strong overlap in OH stretching zone. The addition of nanocellulose had no major influence on the molecular structure of PVA. Fig. 6. (a) shows the peaks for different combinations of PVA/CNC concentrations.



(a) (b)

Fig. 6. (a) FTIR spectra for PVA-CNC film samples with varying compositions; (b) XRD spectra for different PVA-CNC film samples

XRD: CNC exhibited four characteristic peaks at 14.7° ((101) plane), 16.5° ((10$\bar{1}$) plane), 20.4° ((102) plane), and 22.7° ((200) plane). In contrast, PVA showed a peak at 19.5°, attributed to hydrogen bonding between polymer chains and its semicrystalline structure (Popescu et al., 2018). All PVA/nanocellulose composite films displayed the characteristic PVA peak at 19.5°, corresponding to the (110) plane of partially hydrolysed PVA, indicating that the crystal structure of PVA was retained even after CNC incorporation. However, with increasing CNC content, the intensity of the 19.5° peak decreased, while the 22.7° peak became more prominent. Fig.6.(b) shows the diffraction patterns of the control films. Films 5P1C and 5P2C exhibited distinct peaks for both CNC and PVA, whereas the CNC peak was less prominent in 6P1C and 6P2C films. This may be due to less uniform mixing and weaker bond formation between CNC and PVA at higher PVA concentrations. A possible reason for this is chain agglomeration and thus reduced crystallinity (Visakh & Nazarenko, 2023). At lower PVA concentrations, crystallinity increased with CNC addition, but decreased again at 6% PVA concentration.

3.2.2 Mechanical properties

CNC is responsible for higher crystallinity and hardness of the film, and the polymer is responsible for flexibility and ductility. Films with higher CNC content tend to have higher TS and brittleness. Table 2. Shows the mechanical properties of different samples. Fig. 8 depicts the TS and flexibility for different films, with film 5P1C giving the best result in terms of flexibility and strength, balancing both with Young's modulus of 16.75, as shown in the table. Film 6P2C gave the highest strength, but as the stress-strain curve shows, it was brittle. This could be attributed to strong hydrogen bonding between PVA and CNC, resulting in a very compact structure that leaves less room for chain mobility (Visakh & Nazarenko, 2023). Film 6P also exhibited good flexibility, but the Young's modulus was compromised. PVA, when used at higher concentrations, can demonstrate good TS because the polymer chains are tightly bound and have a low degree of flexibility (Popescu et al., 2018). Young's modulus is the measure of a material's stiffness. We can, therefore, comment that the addition of CNC to PVA can improve the Young's modulus by as much as 87 %, as is demonstrated by (Zhang et al., 2018). Film 5P1C is the ideal among all samples for packaging applications, depicting desirable strength, elongation and stiffness.

Table 2: Mechanical properties of the PVA-CNC film samples

S.No	Sample	Young's modulus	TS	Eb%
1	5P	3.51	15.14	237
2	6P	6.085	33.357	144.628
3	5P1C	16.75	47.9	116
4	6P1C	21.05	54	47
5	5P2C	19.03	54.6	95
6	6P2C	27.51	77.6	102

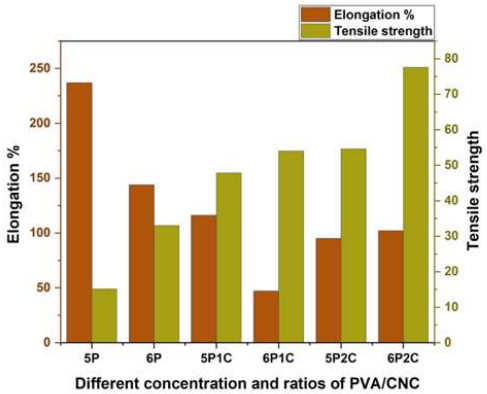
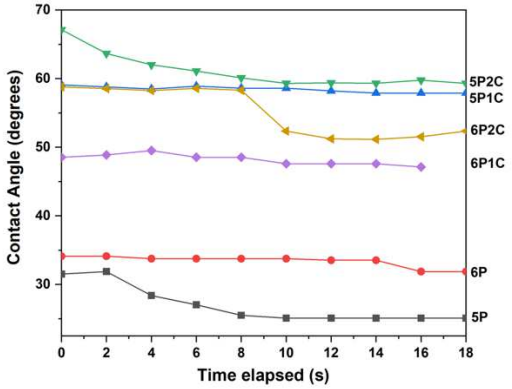


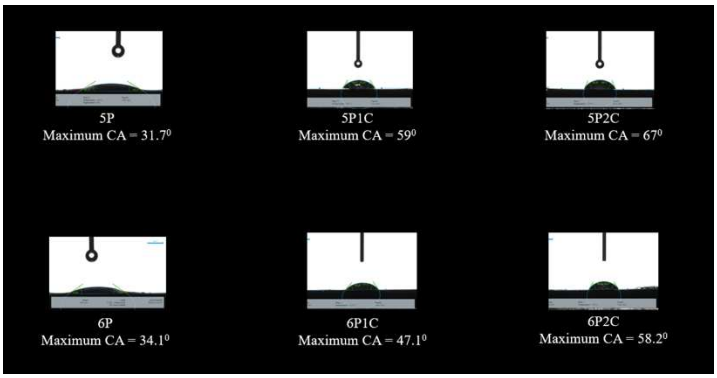
Fig 8: Tensile strength (TS) and Elongation % (Eb) for films with different concentrations and ratios of PVA and CNC

3.2.3 Contact angle analysis

Hydrophobicity is one of the most required properties when it comes to packaging films. Moisture resistance is required to maintain the longer shelf life of food. Nanocellulose is hydrophilic due to the presence of excess hydroxyl groups, and so is PVA (Bai et al., 2022). However, when mixed properly, these can form very strong and compact structures due to rigid hydrogen bonding that takes place between the two. As shown in Fig. 9, the contact angles recorded for the nanocomposite films were higher than those for pure PVA, with values increasing as the CNC content rose. It has been demonstrated before by (Jose et al., 2015), that the better the diffusibility of a nano-filler in a polymeric matrix, the greater the reduction in wettability. The physical bonding between the polymer matrix and the surface groups present in the nano-filler is the possible reason. The highest contact angle was observed in the composite film containing 5% PVA and 2% CNC, but the film was quite brittle, as mentioned in the section for mechanical properties. Films 6P2C and 5P2C showed appreciable hydrophobicity contact angles, but also higher absorption. In the literature, it has been demonstrated that higher CNC concentration or any additive may result in saturation of the base matrix, leading to possible agglomeration and phase separation, which can in turn result in lower surface energy (Kim et al., 2007). According to the given data, 5P1C exhibits ideal wettability for a PVA-CNC film, with no visible absorption over time.



(a)



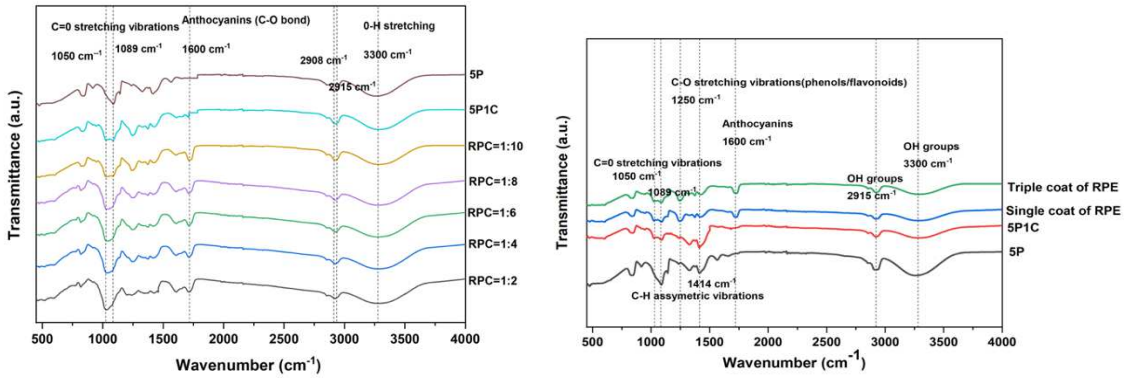
(b)

Fig. 9. (a): Contact angle variation exhibited by PVA-CNC films; (b) Images depicting the highest contact angles recorded while drop-casting

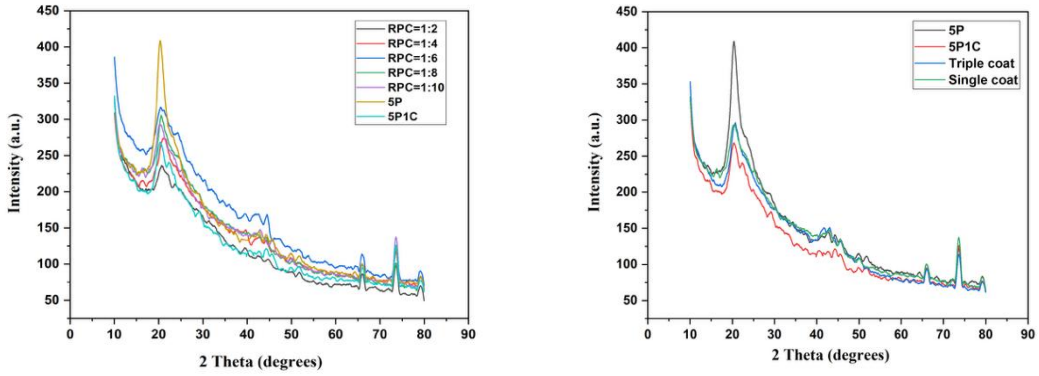
3.3 For RPE films

3.3.1 Structural analysis

FTIR: RPE disrupts hydrogen bonding within molecules, affecting their chemistry. The notable band at 1607 cm-1 indicates C=O bond stretching in anthocyanins, becoming more prominent with higher RPE content (De Abreu et al., 2021). As RPE increases, the OH stretching peak shifts to a higher wavelength due to phenolic OH groups. The absorption band at 1430 cm-1, related to symmetric CH_2 bending, diminishes. Films with minimal RPE resemble the control, featuring O-H stretching vibrations around 3300 cm-1 for PVA and 3327 cm-1 for CNC; these bands merge into approximately 3280 cm-1 in composite films. The band at ~1089 cm^{-1}, representing C–O stretching from PVA and glycosidic linkages from cellulose nanocrystals, decreases with CNC and nearly disappears with RPE due to strong hydrogen bonding with the polymer matrix (Nguyen & Lee, 2023). For coated films, the peak is unchanged as compared with the CNC-PVA film, as the matrix structure has not absorbed the extract, and it's only on the surface, with minimal penetration. The absorption band at ~1414 cm^{-1} reflects CH_2 bending of the PVA backbone, showing slight variations in coated films due to interactions with plant extract's aromatic compounds. Fig. 10. (a) and (b) show the different peaks observed for RPE-blended films and coated films, respectively. Spectra for a single layer of coating resemble the one without coating, except that the coated sample shows the presence of polyphenols at 1600 cm^{-1}. 0H peak at 3300 cm^{-1} is slightly broader for triple coating due to more phenolic hydroxyl groups and bonding with the matrix.



(a) (b)



(c) (d)

Fig.10. (a) FTIR spectra for film samples with RPE incorporated in different ratios in PVA-CNC matrix; (b) FTIR spectra for single-layer and triple-layer of RPE-coated PVA-CNC films; (c) XRD pattern for PVA-CNC films with different ratios of RPE incorporated; (d) XRD analysis for single-layer and triple-layer of RPE-coated over PVA-CNC films.

XRD: Crystallinity degree for control samples, i.e. nanocellulose PVA films, is 68 % and with the introduction of RPE into the matrix, the crystallinity reduces by 33% for the minimum ratio of RPE with the substrate and 45 % for maximum RPE content. As RPE interferes with the internal bonding in the matrix of the nanocomposite, the degree of crystallinity drops. This may be attributed to the interference caused by hydrogen bonding that RPE tries to make with already existing bonding in PVA-CNC (Xu et al., 2019). Because of the possibly disrupted chain alignment and additional free volume created by anthocyanins, the proportion of amorphous regions increases. Fig. 10. (c) and (d) shows the XRD spectra for films with different RPE content.

3.3.2 Mechanical properties

For RPE-incorporated films, Eb% seems to increase with the introduction of RPE, and TS tends to follow a reverse pattern. This is due to the fact that it interferes with the internal bonding and disrupts the intermolecular interactions, leading to a decrease in film strength and an increase in chain mobility. Flexibility increases as the CNC percentage decreases for the same volume of the film-forming solution. Also, RPE has phenolic compounds that tend to form bonds with glucose molecules, which further weaken the intermolecular forces present among the polymer chains, resulting in a higher degree of freedom, so higher flexibility. Highest flexibility was seen for the ratio 1:6, which was considered the optimized content of RPE blended with the matrix, as the TS is also ideal for the application of packaging. Properties again start to diminish with further addition of RPE, due to possible aggregation happening when an excess of RPE saturates the matrix, with no more scope for further bonding. For coated films, results are better in the case of a single coating. For triple coats, the films have become weaker in strength due to absorption of RPE into the matrix and unlike in the case of perfectly blended samples, agglomeration has probably happened in this case, as the RPE has saturated the matrix through absorption, thus interfering with the internal structure. Table. 3 shows different parameters related to the mechanical characteristics of the films, and Fig. 11. depicts the variation in mechanical properties with RPE content via graph.

Table.3. (a) and (b): Mechanical properties for RPE incorporated and RPE-coated PVA-CNC films, respectively

(a)

S.No	Sample	Young's modulus	TS	Eb%
1	5P	6.39	15.14	237

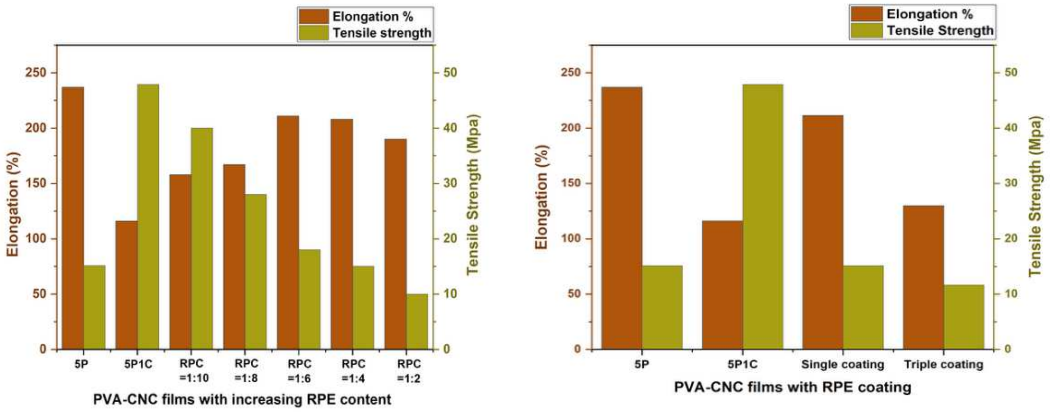
2	5P1C	41.29	47.9	116
3	RPC=1:10	25.32	40	158
4	RPC=1:8	16.77	28	167
5	RPC=1:6	8.53	18	211
6	RPC=1:4	7.21	15	208
7	RPC=1:2	5.26	10	190

384

385 (b)

S.No	Sample	Young's modulus	TS	Eb%
1	Single coating	7.55	16	212
2	Triple coating	8.03	11	137

386



387

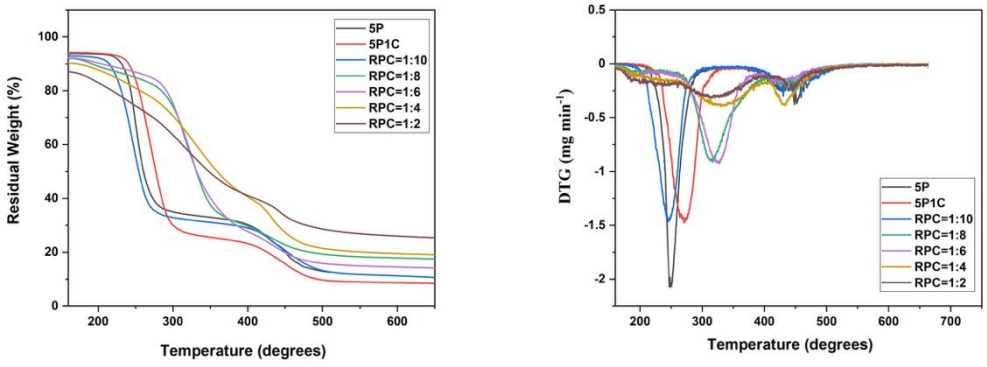
388 (a) (b)

389 Fig. 11. (a) and (b) Variation in mechanical properties with different ratios of RPE added into the PVA-CNC film
390 matrix and different layers of RPE coated over the films, respectively.

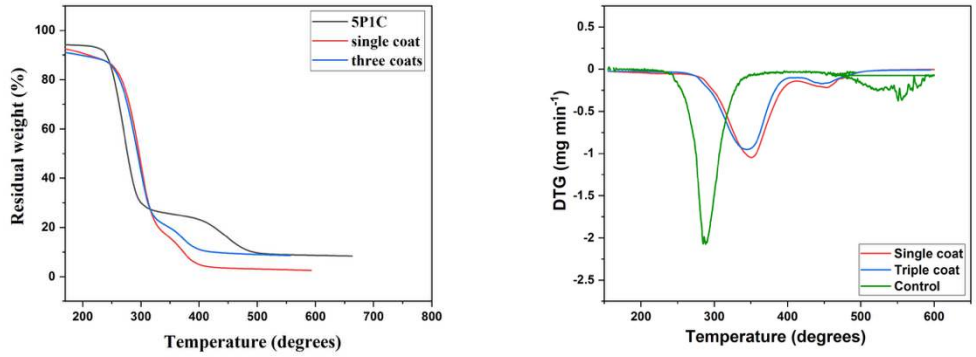
391 **3.3.3 Thermal properties**

TGA and DTG analysis of the blended films is shown in Fig. 12 (a) and (b), respectively. Table 4 (a) presents the onset temperature for degradation (T_{onset}) and T_{10} and T_{50}, which represent the temperatures at which 10% and 50% degradation has occurred, respectively. PVA exhibited three thermal degradation stages in the range of 30 °C to 600 °C, which is consistent with previous reports (Tripathi et al., 2009). Degradation happening below 160 °C is due to loosely bound water molecules. PVA/CNC films showed a similar thermal degradation pattern with slightly better thermal resistance, which may be attributed to strong hydrogen bonding between PVA and CNC. T_{onset} starts decreasing as RPE is introduced in the films, with the lowest T_{onset} at the highest ratio of RPE. This is the loosely bound moisture that goes away first. Although the rate of degradation is much slower in RPE films compared with neat PVA and PVA/CNC films, but after a certain temperature. As the RPE content increases, the rate of degradation slows down, with the film RPC=1:2 exhibiting the lowest degradation rate. Below around 260 °C, the rate of degradation increases with RPE content. In contrast, when the temperature was above 260 °C, the thermal resistance of PVA/CNC/RPE films increased. These results were consistent with (Nguyen & Lee, 2023). The incorporation of plant extract lead to a decrease in the onset degradation temperature due to the presence of thermally less stable low-molecular-weight components. However, the overall degradation rate was reduced, which can be due to the presence of thermally stable aromatic structures. There are mainly 4 stages of the degradation cycle of PVA/CNC/RPE films: (1) below 160 °C (degradation of loosely bound water molecules) (2) 160 °C – 250 °C (partial thermal decomposition of RPE), (2) 230 °C – 400 °C (thermal decomposition of PVA, CNCs and polyphenolic compounds present in RPE), and (3) above 400 °C (thermal decomposition of residual char) (De Abreu et al., 2021).

As depicted in Fig. 12 (c) and (d) and Table 6 (b), for coated films, the degradation temperatures are almost the same. The only difference is that once 90 % degradation has happened, the pace of further degradation has slowed down for the triple-coated film than for the single-coated film.



(a) (b)



(c) (d)

Fig. 12. (a) TGA analysis; (b) DTG analysis for PVA-CNC films with different ratios of RPE incorporated, depicting their thermal stability; (c) TGA analysis, (d) DTG analysis for RPE-coated PVA-CNC films.

Table. 4. (a) Different PVA-CNC films displaying degradation temperatures based on incorporated RPE content; (b) Degradation temperatures for RPE-coated PVA-CNC films

Films	T_{onset}	T_{10}	T_{50}
5P	229.85	249.64	276.04
5P1C	233.94	248.70	283.69
RPC=1:10	212	229.75	262
RPC=1:8	188	278.37	342.43
RPC=1:6	190	279	338.50
RPC=1:4	189.87	245	332.45
RPC=1:2	175	218	378.61

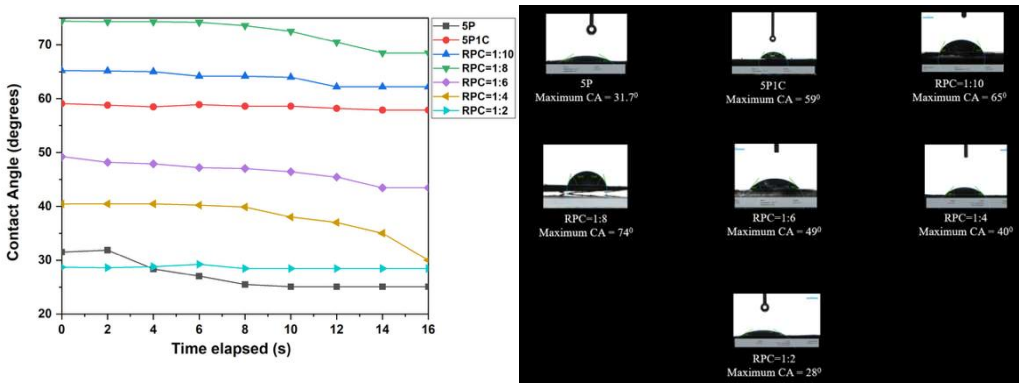
(a)

Films	T_{onset}	T_{10}	T_{50}
5P1C	233.94	248.70	283.69
Single coating	246.2	276	312
Triple coating	246	273	311

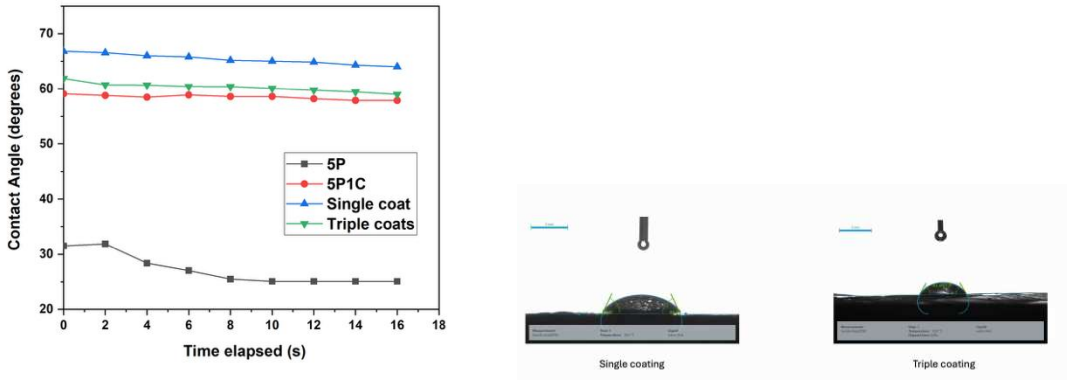
(b)

3.3.4 Contact angle analysis

Rose petals contain waxes and phenols, making their surface superhydrophobic. As shown in Fig. 13 (a), increasing RPE content in the film matrix raises the contact angle, indicating greater hydrophobicity, and the straight lines suggest little water absorption over time. Pure PVA and PVA-CNC films have excess OH groups, thus resulting in high surface energy and hydrophilic surfaces (Barbălată-Mândru et al., 2022). The highest contact angle occurs for the film with a ratio of 1:8, after which it decreases with further addition of RPE, likely due to phase separation or agglomeration happening at high RPE content (Silva et al., 2021), which results in unbonded OH groups and thus, reduced hydrophobicity. Fig 13 (b) presents the maximum contact angles obtained for the samples. For coated films, as evident in Fig. 13 (c), both samples depict better hydrophobicity than the control samples, demonstrating the effectiveness of the extract in modifying surface wettability. The triple-coated film shows a smaller contact angle than the singly-coated film, indicating that three coats have made the film more susceptible to moisture by exposing more phenol groups (-OH, sugar moieties, -COOH) on the surface.



(a) (b)



(c) (d)

Fig. 13. (a) Change in contact angle with time, depicting absorption of water for RPE incorporated PVA-CNC films; (b) Images showing maximum contact angle obtained for the samples while drop-casting; (c) Change in contact angle with time for RPE-coated PVA-CNC films; (d) Images for maximum contact angle obtained during drop casting for coated film samples.

3.3.5 Water vapour transmission rate (WVTR)

To efficiently regulate moisture transfer into and out of packaging films and help maintain the proper moisture content (MC) of foods, the WVTR of the films should be kept to a minimum (Van Nguyen & Lee, 2023). As shown in Table 5, WVTR is lowest for 5P1C. Since nanocellulose has a higher crystallinity, it results in providing rigidity to the hydrogen-bonded network, leading to an increase in tortuosity (Nguyen & Lee, 2022). WVTR is affected greatly after RPE introduction, initially increasing, which may be due to the disturbance caused in the compact molecular structure of the matrix, probably resulting more porosity. Blending the extract into the polymer matrix disrupts intermolecular interactions, increases free volume, and promotes phase separation, thereby facilitating better water vapor permeation. But, as RPE content is increased, there is a decrease in the value of WVTR encountered again. The intermolecular spacing present in the films is reduced, thus decreasing the transmission rate. For coated samples, a considerably lower WVTR was recorded for a single-coated film, probably due to the formation of a continuous surface barrier layer enriched with phenolic compounds; the moisture diffusion is restricted at the very surface. But this is further increased for triple coats as the base matrix absorbs RPE coated on it and disrupts the internal structure.

Table. 5.(a). WVTR for PVA-CNC films with different RPE ratios incorporated. (b) Shows WVTR for single-layer and triple-layer RPE-coated PVA-CNC film samples

Films	WVTR ($g/m^2.day$)
5P	160.90
5P1C	33.34
RPC=1:10	42.59
RPC=1:8	39.21
RPC=1:6	31.88
RPC=1:4	23.29
RPC=1:2	12.76

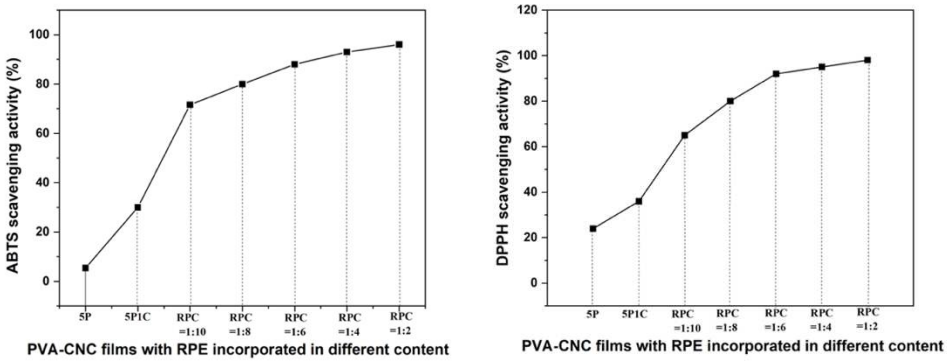
(a)

Films	WVTR ($g/m^2.day$)
Single coating	21.7302
Triple coating	39.2376

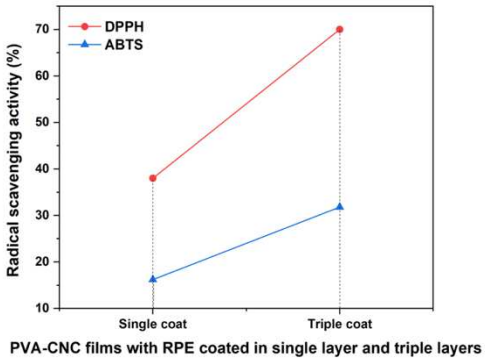
(b)

3.3.6 Antioxidant activity

Radicle scavenging has become a desirable trait as free radicals initiate chain oxidation of lipids, thus inducing food spoilage. RPE has anthocyanins, which are natural antioxidants (Yontar & Çevik, 2023). The presence of phenols and flavonoids is responsible for radical scavenging, and these compounds also chelate metal ions, thus protecting the system from lipid peroxidation (Rambabu et al., 2019). Phenolics are certain chemical groups that are made up of one or more aromatic rings when present with hydroxyl groups. As depicted in the data in Fig. 14(a), antioxidant potential is rising with increasing RPE content for both DPPH and ABTS, with the highest, 98 % radical scavenging obtained for the highest ratio of RPE in the case of the DPPH test and 96 % in the case of the ABTS assay. Neat PVA film showed 24 % and 5.37 % antioxidant potential for DPPH and ABTS, respectively and 5P1C film showed 36 % and 37 % activity for the same, respectively. For coated films, as shown in Fig. 14(b), the inhibition was better for triple-coated films for both ABTS and DPPH.



(a)



(b)

Fig. 14. (a) ABTS and DPPH radical scavenging activity (%) for RPE incorporated PVA-CNC film samples; (b) DPPH and ABTS radical inhibition (%) for RPE coated PVA-CNC film samples.

4. Conclusion and Future Prospects:

In this work, plant extract incorporated and coated food packaging films have been developed, which show improved barrier, mechanical and acquired antioxidant properties. The flexibility of the films was improved with RPE administration, and radical scavenging was also noticeable. The solvent casting method was employed for producing the films, and these were analyzed on the basis of different characterization techniques. In comparison with control samples, which were neat PVA and PVA-CNC films, RPE-administered films exhibited better hydrophobicity and WVTR, with the ratio RPC=1:6 performing the best overall. However, on further addition of the extract, the properties were again compromised, probably due to agglomeration and phase separation happening due to saturation of RPE into the base matrix. Furthermore, Shelf-life analysis shall be conducted on the prepared films to assess how effective they are in actually suppressing food spoilage. Also, life cycle assessment (LCA) studies shall be done to check if their production process is environmentally sound, to pave the way for scaling up the process in future.

Acknowledgements

The authors are grateful for the financial support provided by the Indian Institute of Technology, Delhi and characterization facilities provided by the Central Research Facility (CRF) and Nanoscale Research Facility (NRF) at IIT Delhi.

Authors' Contributions

Urvashi Singh: Writing – original draft, conceptualization, methodology, investigation, formal analysis, data curation and visualization

Madan Kumar: Writing – review & editing and validation

Vivek Kumar: Supervision, project administration and resources.

S.K.Khare: Supervision

Data Availability

No datasets were generated or analysed during the current study.

Declarations

Competing Interests: The authors declare no competing interests.

References

1. Amara, C., El Mahdi, A., Medimagh, R., & Khwaldia, K. (2021). Nanocellulose-based composites for packaging applications. In *Current Opinion in Green and Sustainable Chemistry* (Vol. 31). https://doi.org/10.1016/j.cogsc.2021.100512
2. ASTM E96/E96M-22: Standard Test Methods for Gravimetric Determination of Water Vapor Transmission Rate of Materials, ASTM International (2022).
3. Bai, H., Li, Y., Zhang, S., Ma, P., & Dong, W. (2022). Photo-crosslinkable poly (vinyl alcohol)/nanocrystalline cellulose composites with controllable performance and exceptional water vapor barrier property for packaging application. *Cellulose*, *29*(14), 7721–7734. https://doi.org/10.1007/s10570-022-04760-x
4. Bhushan, B., & Nosonovsky, M. (2010). The rose petal effect and the modes of superhydrophobicity. *Philosophical Transactions of the Royal Society A: Mathematical, Physical and Engineering Sciences*, *368*(1929). https://doi.org/10.1098/rsta.2010.0203
5. Chakrabarty, A., & Teramoto, Y. (2018). Recent advances in nanocellulose composites with polymers: A guide for choosing partners and how to incorporate them. In *Polymers* (Vol. 10, Number 5). https://doi.org/10.3390/polym10050517
6. De Abreu, D. A. P., Rodriguez, K. V., & Cruz, J. M. (2021). Development of antioxidant active PVA films with plant extract of Caesalpinia ferrea Martius. *LWT*, *144*(JANUARY), 111215. https://doi.org/10.1016/j.ifset.2011.10.003
7. Ghaderi, M., Mousavi, M., Yousefi, H., & Labbafi, M. (2014). All-cellulose nanocomposite film made from bagasse cellulose nanofibers for food packaging application. *Carbohydrate Polymers*, *104*(1). https://doi.org/10.1016/j.carbpol.2014.01.013
8. Guzman-Puyol, S., Hierrezuelo, J., Benítez, J. J., Tedeschi, G., Porras-Vázquez, J. M., Heredia, A., Athanassiou, A., Romero, D., & Heredia-Guerrero, J. A. (2022). Transparent, UV-blocking, and high barrier cellulose-based bioplastics with naringin as active food packaging materials. *International Journal of Biological Macromolecules*, *209*. https://doi.org/10.1016/j.ijbiomac.2022.04.177
9. Hasan, Md. M., Abu Nayem, K., Anwarul Azim, A. Y. M., & Ghosh, N. C. (2015). Application of Purified Lawsone as Natural Dye on Cotton and Silk Fabric. *Journal of Textiles*, *2015*. https://doi.org/10.1155/2015/932627
10. He, X., Lu, W., Sun, C., Khalesi, H., Mata, A., Andaleeb, R., & Fang, Y. (2021). Cellulose and cellulose derivatives: Different colloidal states and food-related applications. *Carbohydrate Polymers*, *255*, 117334. https://doi.org/10.1016/J.CARBPOL.2020.117334
11. J. H. Han, & J. M. Krochta. (1999). WETTING PROPERTIES AND WATER VAPOR PERMEABILITY OF WHEY-PROTEIN-COATED PAPER. *Transactions of the ASAE*, *42*(5), 1375–1382. https://doi.org/10.13031/2013.13300
12. Ji, Y., Xu, Q., Jin, L., & Fu, Y. (2020). Cellulosic paper with high antioxidative and barrier properties obtained through incorporation of tannin into kraft pulp fibers. *International Journal of Biological Macromolecules*, *162*. https://doi.org/10.1016/j.ijbiomac.2020.06.101
13. Jose, J., De, S. K., Ma'adeed, M. A. A. Al, Bhadra Dakua, J., Sreekumar, P. A., Sougrat, R., & Al-Harthi, M. A. (2015). Compatibilizing role of carbon nanotubes in poly(vinyl alcohol)/starch blend. *Starch/Staerke*, *67*(1–2). https://doi.org/10.1002/star.201400074

14. Kanatt, S. R. (2021a). Active/smart carboxymethyl cellulose-polyvinyl alcohol composite films containing rose petal extract for fish packaging. *International Journal of Food Science and Technology*, *56*(11). https://doi.org/10.1111/ijfs.15095
15. Kanatt, S. R. (2021b). Active/smart carboxymethyl cellulose-polyvinyl alcohol composite films containing rose petal extract for fish packaging. *International Journal of Food Science & Technology*, *56*(11), 5753–5761. https://doi.org/10.1111/ijfs.15095
16. Kasaai, M. R., & Moosavi, A. (2017). Treatment of Kraft paper with citrus wastes for food packaging applications: Water and oxygen barrier properties improvement. *Food Packaging and Shelf Life*, *12*. https://doi.org/10.1016/j.fpsl.2017.02.006
17. Khwaldia, K. (2010). Water Vapor Barrier And Mechanical Properties Of Paper-Sodium Caseinate And Paper-Sodium Caseinate-Paraffin Wax Films. *Journal of Food Biochemistry*, *34*(5). https://doi.org/10.1111/j.1745-4514.2010.00345.x
18. Kim, J. H., Shin, D. S., Han, M. H., Kwon, O. W., Lee, H. K., Lee, S. G., Ghim, H. Do, Park, J. M., Han, S. S., Noh, S. K., & Lyoo, W. S. (2007). Surface free energy analysis of poly(vinyl alcohol) films having various molecular parameters. *Journal of Applied Polymer Science*, *105*(2), 424–428. https://doi.org/10.1002/app.26010
19. Kusmono, Listyanda, R. F., Wildan, M. W., & Ilman, M. N. (2020). Preparation and characterization of cellulose nanocrystal extracted from ramie fibers by sulfuric acid hydrolysis. *Heliyon*, *6*(11). https://doi.org/10.1016/j.heliyon.2020.e05486
20. Liu, Y., Ahmed, S., Sameen, D. E., Wang, Y., Lu, R., Dai, J., Li, S., & Qin, W. (2021). A review of cellulose and its derivatives in biopolymer-based for food packaging application. *Trends in Food Science & Technology*, *112*, 532–546. https://doi.org/10.1016/J.TIFS.2021.04.016
21. Nagy, Á., & Kuti, R. (2016). The Environmental Impact of Plastic Waste Incineration. *Academic and Applied Research in Military and Public Management Science*, *15*(3). https://doi.org/10.32565/aarms.2016.3.3
22. Nguyen, S. Van, & Lee, B. K. (2022). PVA/CNC/TiO2 nanocomposite for food-packaging: Improved mechanical, UV/water vapor barrier, and antimicrobial properties. *Carbohydrate Polymers*, *298*, 120064. https://doi.org/10.1016/J.CARBPOL.2022.120064
23. Nguyen, S. Van, & Lee, B. K. (2023). Multifunctional nanocomposite based on polyvinyl alcohol, cellulose nanocrystals, titanium dioxide, and apple peel extract for food packaging. *International Journal of Biological Macromolecules*, *227*(21), 551–563. https://doi.org/10.1016/j.ijbiomac.2022.12.073
24. Oksman, K., & Sain, M. (2016). Cellulose Nanocomposites, Processing, Characterization and Properties. *ACS Symposium Series*, *938*.
25. Phanthong, P., Reubroycharoen, P., Hao, X., Xu, G., Abudula, A., & Guan, G. (2018). Nanocellulose: Extraction and application. In *Carbon Resources Conversion* (Vol. 1, Number 1). https://doi.org/10.1016/j.crcon.2018.05.004
26. Popescu, M. C. (2017a). Structure and sorption properties of CNC reinforced PVA films. *International Journal of Biological Macromolecules*, *101*, 783–790. https://doi.org/10.1016/J.IJBIOMAC.2017.03.168
27. Popescu, M. C. (2017b). Structure and sorption properties of CNC reinforced PVA films. *International Journal of Biological Macromolecules*, *101*(5), 783–790. https://doi.org/10.1016/j.ijbiomac.2017.03.168
28. Popescu, M. C., Dogaru, B. I., Goanta, M., & Timpu, D. (2018). Structural and morphological evaluation of CNC reinforced PVA/Starch biodegradable films. *International Journal of Biological Macromolecules*, *116*(12), 385–393. https://doi.org/10.1016/j.ijbiomac.2018.05.036

29. Rambabu, K., Bharath, G., Banat, F., Show, P. L., & Cocoletzi, H. H. (2019). Mango leaf extract incorporated chitosan antioxidant film for active food packaging. *International Journal of Biological Macromolecules*, *126*, 1234–1243. https://doi.org/10.1016/J.IJBIOMAC.2018.12.196
30. Selvam, T., Rahman, N. M. M. A., Olivito, F., Ilham, Z., Ahmad, R., & Wan-Mohtar, W. A. A. Q. I. (2025). Agricultural Waste-Derived Biopolymers for Sustainable Food Packaging: Challenges and Future Prospects. *Polymers*, *17*(14), 1897. https://doi.org/10.3390/polym17141897
31. Sharma, B. K., Jha, A., Bhalani, D., Pillai, S. A., Pal, S., Patil, K., & Nagaraj, K. (2026). Advancements in Bioresource-based Polymers and Composites: Sustainable Alternatives to Non-biodegradable Plastics for a Greener Future: A Review. *Current Green Chemistry*, *13*(2), 163–182. https://doi.org/10.2174/0122133461372269250503082219
32. Tripathi, S., Mehrotra, G. K., & Dutta, P. K. (2009). Physicochemical and bioactivity of cross-linked chitosan–PVA film for food packaging applications. *International Journal of Biological Macromolecules*, *45*(4), 372–376. https://doi.org/10.1016/J.IJBIOMAC.2009.07.006
33. Ulaganathan, R. K., Mohamad Senusi, N. A., Mohd Amin, M. A., Abdul Razab, M. K. A., Ismardi, A., & Abdullah, N. H. (2022). Effect of cellulose nanocrystals (CNC) on PVA/CNC bio-nanocomposite film as potential food packaging application. *Materials Today: Proceedings*, *66*, 3150–3153. https://doi.org/10.1016/J.MATPR.2022.07.466
34. Van Nguyen, S., & Lee, B.-K. (2023). Multifunctional food packaging polymer composites based on polyvinyl alcohol/cellulose nanocrystals/apple peel extract. *Cellulose*, *30*(3), 1697–1716. https://doi.org/10.1007/s10570-022-04976-x
35. Xu, T., Gao, C. C., Feng, X., Yang, Y., Shen, X., & Tang, X. (2019). Structure, physical and antioxidant properties of chitosan-gum arabic edible films incorporated with cinnamon essential oil. *International Journal of Biological Macromolecules*, *134*, 230–236. https://doi.org/10.1016/J.IJBIOMAC.2019.04.189
36. Yogalakshmi, K. N., & Singh, S. (2020). Plastic Waste: Environmental Hazards, Its Biodegradation, and Challenges. In *Bioremediation of Industrial Waste for Environmental Safety*. https://doi.org/10.1007/978-981-13-1891-7_6
37. Yontar, A. K., & Çevik, S. (2023). Effects of Plant Extracts and Green-Synthesized Silver Nanoparticles on the Polyvinyl Alcohol (PVA) Nanocomposite Films. *Arabian Journal for Science and Engineering*, *48*(9), 12043–12060. https://doi.org/10.1007/s13369-023-07643-w
38. Zhang, J., Lei, W., Chen, J., Liu, D., Tang, B., Li, J., & Wang, X. (2018). Enhancing the thermal and mechanical properties of polyvinyl alcohol (PVA) with boron nitride nanosheets and cellulose nanocrystals. *Polymer*, *148*(34), 101–108. https://doi.org/10.1016/j.polymer.2018.06.029